Tuning the Magnetocaloric Properties of the La(Fe,Si)13 Compounds by Chemical Substitution and Light Element Insertion

Valérie Paul-boncour, Lotfi Bessais

magnetochemistry

MDPI

Article

Tuning the Magnetocaloric Properties of the La(Fe,Si)$_{13}$ Compounds by Chemical Substitution and Light Element Insertion

Valérie Paul-Boncour * and Lotfi Bessais

Univ Paris Est Creteil, CNRS, ICMPE, UMR 7182, 2 rue Henri Dunant, 94320 Thiais, France; bessais@icmpe.cnrs.fr
* Correspondence: paulbon@icmpe.cnrs.fr; Tel.: +33-1-4978-1207

Abstract: $LaFe_{13-x}Si_x$ compounds exhibit a giant magnetocaloric effect and they are considered as a good magnetocaloric working substance for an environmentally friendly cooling technique. Nevertheless as the Curie temperature T_C is around 200 K, it is necessary to tune T_C near room temperature for magnetic refrigeration. In this work we present a review of the various methods of synthesis and shaping of the $LaFe_{13-x}Si_x$ type compounds as well as the influence of chemical substitution, light element insertion or combination of both on T_C, magnetic entropy and adiabatic temperature variation (ΔS_M and ΔT_{ad}), and stability upon cycling. The advantages and drawbacks of each method of preparation and type of element substitution/insertion are discussed. The implementation of these $NaZn_{13}$ type materials in active magnetic refrigerator is presented and their performances are compared to that of Gd in prototypes.

Keywords: intermetallics; $NaZn_{13}$ compounds; magnetocaloric effect; magnetic refrigeration

Citation: Paul-Boncour, V.; Bessais, L. Tuning the Magnetocaloric Properties of the La(Fe,Si)$_{13}$ Compounds by Chemical Substitution and Light Element Insertion. *Magnetochemistry* **2021**, *7*, 13. https://doi.org/10.3390/magnetochemistry7010013

Received: 15 December 2020
Accepted: 12 January 2021
Published: 14 January 2021

1. Introduction

Classical refrigeration technologies are using refrigerants that deplete the ozone layer and contribute to global warming, and will be therefore forbidden by different climate protocols. Alternative refrigerants present also various drawbacks (flammable, toxic). Therefore, it is worth developing new refrigeration technologies without environmental problems [1,2], such as magnetic refrigeration that is based on the magnetocaloric effect. The development of efficient magnetocaloric materials has become challenging since the discovery of a giant magnetocaloric effect (MCE) near room temperature (RT) in $Gd(Ge,Si)_5$, $MnAs_{1-x}Sb_x$ and FeRh based alloys [3–11].

Since that time, intensive studies have yielded the discovery of several families of materials, among which the La(Fe,Si)$_{13}$ system, which displays a giant magnetocaloric effect, and is considered as a good magnetocaloric material for magnetic refrigeration. This system is particularly interesting, because it has relatively cheap, abundant, and non-toxic constituents. However several questions should be solved to use this material for magnetic refrigeration: (i) the synthesis and shaping of the material should be fast, not too expensive, and appropriate for an industrial scaling, (ii) the chemical composition should be adjusted to reach room temperature, as La(Fe,Si)$_{13}$ Curie temperature is close to 200 K, while keeping a giant MCE effect, and (iii) the compounds should remain stable upon a large number of thermomagnetic cycles. In this paper, we first propose a review of the main works that have been undertaken to solve these different challenges. The different methods of synthesis and shaping will be presented and then compared. The influence of both chemical substitution of La, Fe, and Si by other elements as well as the insertion of light elements (H, C) will be presented to show the advantages and drawbacks of each solutions.

We have developed a synthesis method combining high energy ball milling with a subsequent short annealing treatment in order to obtain a single-phase compound. Besides, a reactive Spark Plasma Sintering (SPS) method has been used in order to produce and

sinter a powdered sample in one single step. The carbon atoms were inserted by solid/solid reaction, while the hydrogenation of the parent intermetallic La(Fe,Si,Co)$_{13}$ alloys was carried out using a Sievert method. A study of our own experimental results will then be presented, which combines Fe for Co substitution with the hydrogen insertion in order to give an example of a strategy developed to obtain performant magnetocaloric materials. The insertion of light elements (H, C) or/and cobalt for iron substitution are used in order to improve the Curie temperature near room temperature for magnetic refrigeration applications. The tuning of the Curie temperature is explained by a combination of the structural and electronic properties. The advantages and disadvantages of each type of element insertion are discussed and the misunderstanding on interstitial site is clarified.

2. Sample Synthesis

Condition of Synthesis of La($Fe_{1-X}Si_x$)$_{13}$ Type Alloys

Contrary to LaCo$_{13}$, the binary LaFe$_{13}$ compound does not form, but the 1:13 phase can be stabilized by a partial Si for Fe substitution. The study of the ternary La-Fe-Si ternary phase diagram at 1173, 1373, and 1573 K [12,13] showed that the LaFe$_{13-x}$Si$_x$ compounds only exist in a very narrow range of composition (with La/(Fe+Si) =1/14) and crystallize either in the cubic NaZn$_{13}$ type structure (phase τ_1) or the tetragonal $Ce_2Ni_{17}Si_9$-type structure (phase τ_2). At 1200 K, τ_1 is single phase for $0.08 \leq x \leq 0.21$ and τ_2 for $0.25 \leq x \leq 0.40$. Both of the phases coexist between 0.21 and 0.25. The Si concentration at the boundaries varies with the equilibrium temperature. The NaZn$_{13}$ phase forms via a peritectic reaction at $T = 1665$ K:

$$L_{FeSi} + L_{La} + LaFe_2Si_2 \rightarrow \tau_1 \quad \text{or} \quad \alpha - Fe + L_{La} + LaFe_2Si_2 \rightarrow \tau_1$$

The as-cast alloys are constituted by a mixture of $\alpha-$Fe(Si) and LaFeSi (formed from the liquid L_{La} phase upon cooling) and an appropriate thermal treatment is necessary for obtaining the NaZn$_{13}$ τ_1-phase via a diffusion process [14–16]. The single phase NaZn$_{13}$ samples can be synthesized by arc or induction melting with a further annealing treatment at temperatures between 1273 and 1423 K and during several days or weeks [11,12]. It is necessary to take the risk of La oxidation into account and an excess of La is generally added in order to avoid the formation of secondary phases [17]. The chemical purity of each element, their preparation into a glove box, and the quality of the atmosphere upon melting and annealing (secondary vacuum or Argon pressure) are crucial to obtain single phase compounds. The annealing time can be shortened by increasing the annealing temperature. In ref [18] the NaZn$_{13}$ was obtained for an arc-melted sample annealed 1 h at 1573 K, but some α-Fe was still present. However, in order to prepare a large quantity of sample for magnetic refrigeration application, the too long duration or too high temperature of the annealing treatment remains an economical drawback. Therefore, to reduce the annealing time several alternative synthesis methods have been developed. They are mainly based to a reduction of the grain size and an intimate contact between the various phases obtained as cast to shorten the diffusion path. Among these methods, one can find melt-spinning [19–23], melt extraction [24], drop-tube solidification [25], and solid state sintering [26]. Gas atomization, followed by an annealing treatment of 1 hour at 1323 K, has been developed by Erasteel Company, in order to produce batches of 500 kg of alloys for industrial applications [27]. Another industrial alternative was developed by the Vacuumschmelze Company [28,29], based on powder metallurgy using reactive sintering.

Our group has developed a high energy ball milling method starting with a mixture of LaSi alloys, $\alpha-$Fe and Si. A ball milling of only 1 hour, followed by an annealing treatment of 30 min at 1423 K, were sufficient for obtaining 95 % of the NaZn$_{13}$ phase with very small quantities of $\alpha-$(Fe,Si), La_2O_3 and La(OH)$_3$ [30]. A comparison of the results that were obtained by these different techniques can be found in [31].

Furthermore, it is also necessary to shape the magnetocaloric material in appropriate form as a function of the design of the magnetic refrigeration device. Several methods have been investigated, like extrusion after mixing with an epoxy polymer [27], thermal

decomposition and recombination (TDR) process [29], and selective laser melting [32]. Erasteel has been chosen to mix the powder that was obtained from gas atomization with epoxy, whereas Vacuumschmelze has developed the TDR process in order to shape their materials in specific form. They prepare an alloy containing a mixture of $\alpha-$Fe and LaFeSi, which can be easily cut without breaking and then process to the annealing treatment in order to obtain the $NaZn_{13}$ phase.

Our group also succeeded in obtaining a $NaZn_{13}$ sample with a density that is very close to that of bulk sample by combining high energy ball milling with reactive spark plasma sintering (SPS). It was possible to directly obtain the $NaZn_{13}$ phase by sintering the non-annealed BM sample at 1273 K with a heating rate of 100 K/min [31]. The best results were obtained under Ar atmosphere with a final step of 15 min at 1273 K [33].

3. Properties of the $La(Fe_{1-X}Si_x)_{13}$ Compounds

Table 1 reports the crystallographic data of both τ_1 ($NaZn_{13}$) and τ_2 ($Ce_2Ni_{17}Si_9$) phases. The crystal structure of the $NaZn_{13}$ phase is shown in Figure 1. The evolution of the cell parameters versus the Si content have been detailed in [34]. The cubic cell parameter slightly decreases versus Si content ($a \approx 11.46$ Å). The tetragonal distortion corresponds to an expansion along the c axis and an intermediate tetragonal τ_2' phase is found as the distortion progressively increases. The cell volume decrease becomes steeper upon the tetragonal distortion for a Si concentration larger than 20 at.%.

Table 1. Crystallographic data of the $La(Fe,Si)_{13}$ phases [34].

Phase	Pearson	Space Group	Atm.	Wyck.	Sym.	Position
$NaZn_{13}$	cF112	$Fm\bar{3}c$	La	8*a*	432	1/4, 1/4, 1/4
			Fe	8*b*	$m\bar{3}$	0, 0, 0
			Fe, Si	96*i*	*m*..	0, 0.1806, 0.1192
$Ce_2Ni_{17}Si_9$	tI56	$I4/mcm$	La	4*a*	422	0, 0, 1/4
			Fe1	4*d*	*m.mm*	0, 1/2, 0
			Fe2	16*k*	*m*..	0.2024, 0.0691, 0
			Fe3	16*l*	..*m*	0.1294, 0.6294, 0.1832
			Si	16*l**	..*m*	0.33, 0.83, 0.118

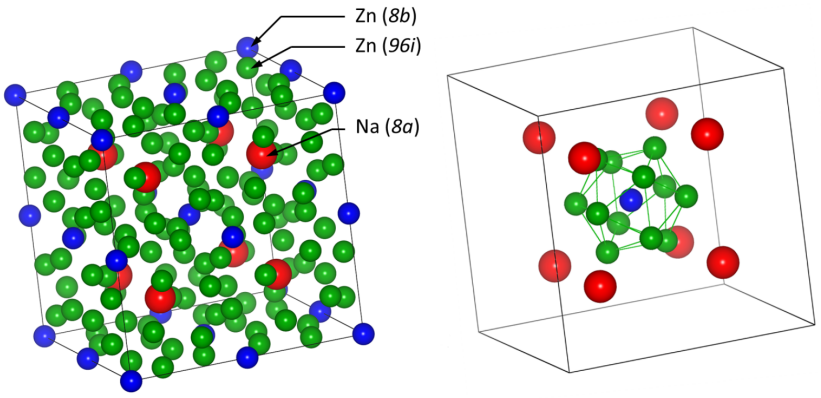

Figure 1. The crystal structure of the cubic $NaZn_{13}$ phase. The La atom occupy the 8*a* sites (Na), whereas the Fe atoms are located on the 8*b* and 96*i* sites (Zn). In the right figure: one Fe (8*b*) atom is surrounded by 10 Fe (96*i*) and 8 La (8*a*). The Si atoms are substituted in the 96*i* position.

All of the $La(Fe_{1-x}Si_x)_{13}$ compounds are ferromagnetic. The Curie temperature T_C monotonously increases from 200 to 260 K for $0.1 < x < 0.21$, and then decreases abruptly reaching 60 K for $x = 0.34$ [34]. The spontaneous magnetization decreases linearly versus Si content with a discontinuity at the $\tau_2' - \tau_2$ transition. The evolution of the magnetic entropy variation ΔS_M at the transition of the τ_1 phase was studied in [30]. It showed that the ΔS_M peak was larger and higher for $x = 0.108$ ($\Delta S_M^{max} = 32.6$ J/kgK) and

broadens progressively as the Si content increases. This indicates a diminution of the first order character of the transition. As the magnetic properties of the τ_2 phase are not suitable for magnetocaloric application and they will not be discussed in the following. Thermal expansion measurements for the τ_1 phase showed that the cell volume decreases sharply at T_C, thus confirming the first order character of the ferromagnetic-paramagnetic transition [35]. Above T_C, an itinerant electron metamagnetic (IEM) behavior is observed. The linear decrease of T_C under applied pressure confirms its strong dependence versus cell volume variation, characteristic of the magnetovolume behavior of IEM compounds.

The $NaZn_{13}$ compounds show hysteresis that yields energy loss upon magnetic cycles due to the first order character of the metamagnetic FM-PM transition. Therefore, several studies have been undertaken in order to reduce the hysteresis [36–39]. It was found that the hysteresis increases with the field sweep rates, but it can be reduced by playing on the sample shape to lower the demagnetization coefficient. Indeed, the hysteresis is smaller for thin or porous samples and fragments when compared to bulk samples. The hysteresis can be also significantly reduced when the applied field is parallel to the smaller dimension of the sample. The presence of local chemical inhomogeneity's also play a role in the local magnetic properties [40].

Therefore, $La(Fe_{1-x}Si_x)_{13}$ compounds with the $NaZn_{13}$ structure are very interesting for their giant magnetocaloric effect and other advantages (moderate cost, environmental friendly), but their Curie temperature remains too low for room temperature magnetic refrigeration. Therefore, many works have been undertaken to reach an operating room temperature range while keeping a giant MCE: the substitution of La or Fe, insertion of light elements (H, C), or combination of both. The main and most interesting results will be described in the following part of this paper.

4. Effect of Iron Substitution in $La(FeSiM)_{13}$ Compounds

The Curie temperature of $La(Fe,Si)_{13}$ alloys was found to be much lower than the $LaCo_{13}$ alloy (1318 K) [41]. The main reason is that Fe-Fe interactions are much weaker than the Co-Co interactions in $NaZn_{13}$-based systems. This fact can explain the increase of T_C in the Co-substituted La-Fe-Si alloys, which was attributed to the strong Co-Fe and Co-Co exchange interactions.

Hu et al. [42], Liu et al. [21], Katter et al. [28], Bjork et al. [43], and Hansen et al. [44] have substituted cobalt for iron atoms, while preserving the first-order magnetic phase transition from paramagnetic to ferromagnetic state at T_C in order to increase the Curie temperature of $LaFe_{13-x}Si_x$. The obtained compound, $LaFe_{11.2}Co_{0.7}Si_{1.1}$ presents a very large magnetic entropy change $\Delta S_M = 20.3\,J/kgK$ under a magnetic field change $\Delta H = 5\,T$ at $T_C = 274\,K$. The main reason of this large ΔS_M is the huge negative lattice expansion at T_C. In addition, the $LaFe_{11.2}Co_{0.7}Si_{1.1}$ compound exhibits a small temperature hysteresis. At the Curie temperature, the unit cell parameter decreases sharply as the structure stay cubic with $Fm\bar{3}c$ space group. The unit cell parameter in the paramagnetic state was smaller than in the ferromagnetic one, with a change of 0.43% for this magnetic state transition.

For $LaFe_{11.2}Si_{1.8}$ compound Hu et al. [45] substituted Fe by Co and studied $La(Fe_{1-x}Co_x)_{11.2}Si_{1.8}$ ($x = 0 - 0.08$) compounds, that they prepared by arc melting and subsequent annealing at 1323 K. They found that the Curie temperature derived from the ZFC-FC magnetization increases from 222 K for $x = 0$ to 307 K for $x = 0.08$, while the magnetic entropy change decreases from 13 J/kg K for $x = 0$ to 8 J/kg K for $x = 0.08$ under magnetic field variation of $0 - 5\,T$. The later value of ΔS_M is just smaller than Gd at the same magnetic field changes $0 - 5\,T$. Another interesting result observed is the disappearance of the field induced itinerant electron metamagnetic transition with cobalt content; indeed, Hu et al. [45] underlined that the substitution of iron by cobalt induced a disappearance of the asymmetrical broadening of ΔS_M peak.

Figure 2 highlights the fact that Si content has much less influence on T_C when considering a Co substituted compound. It shows that the increase of T_C is linear with the substitution rate and it reaches about 310 K for $x = 1$. The increase of T_C is due to

the addition of new 3*d* electrons by the cobalt, which modifies the density of states of the material.

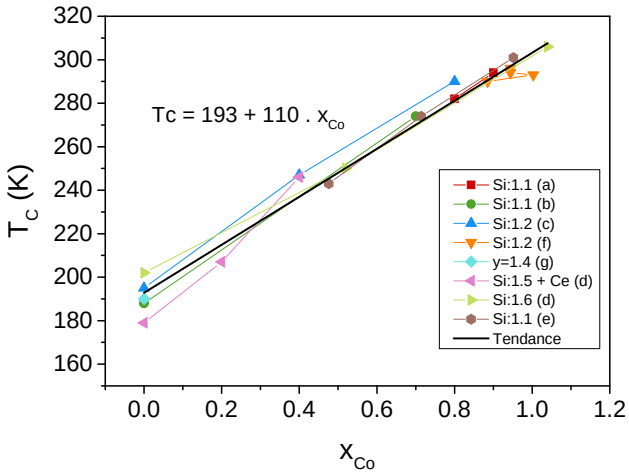

Figure 2. Curie temperature evolution of compounds for which Fe has been partially substituted by Co (a) [46], (b) [47], (c) [48], (d) [49], (e) [18], (f) [50], (g) [21], and (h) [51].

Figure 3 shows a passage from first-order toward second-order magnetic phase transition visible through the quick decrease of ΔS_M^{max} with T_C. An increase in T_C of 100 K due to the Co substitution results in a decrease of ΔS_M^{max} of 13 J/kg.K. The decrease of ΔS_M^{max} is much less than in the case of the silicon content change. Therefore, it is preferable to use Co substitution to increase T_C. The decrease of ΔS_M^{max} due to a second-order transition is compensated by the widening of ΔS_M. In this case, the Relative Cooling Power (RCP) appears to be unchanged. On the other hand, a more spread out transition in working temperature can be efficient for applications.

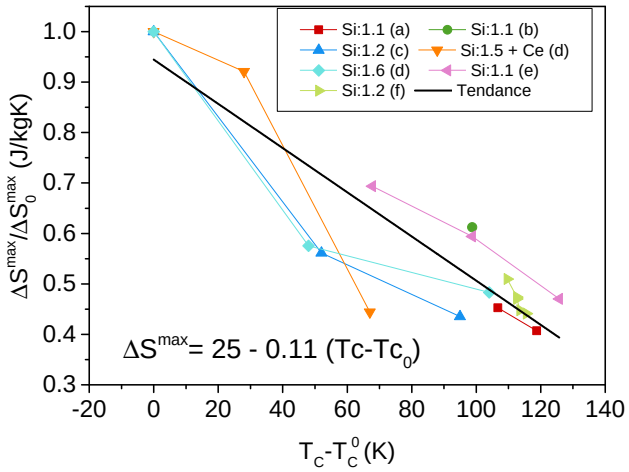

Figure 3. Relative magnetic entropy evolution as a function of T_C for materials in which Fe iron has been substituted by Co, compared to the compound without Co. (a) [46], (b) [47], (c) [48], (d) [49], (e) [18], and (f) [50].

Paul-Boncour et al. [52] studied the influence of cobalt substitution for $LaFe_{11.5-x}Co_xSi_{1.5}$ compounds ($x \leq 2.2$), prepared by ball milling and one of either short annealing treatment or reactive Spark Plasma Sintering (SPS). Their magnetic properties have been investigated while using magnetic measurements, differential scanning calorimetry, and Mössbauer spectroscopy. Figure 4a shows the cell volume at 293 K plotted versus Co content. The annealed and sintered powder display close cell volumes for a given x Co content. We observe a critical range with a cell volume jump, which can be related to the change of

magnetic order, depending on whether samples are above or below T_C, in the ferromagnetic state as the cell volume decreases versus Co content.

The Curie temperature was estimated either from the maxima of dM/dT or dV/dT derivative curves or by the maxima of the DSC peaks. Figure 4b shows the good agreement obtained between these different methods. T_C increases linearly versus x_{Co} content according to the following relation: $T_C = 226 + 97 \times x_{Co}$.

ΔS_M^{max} curves versus temperature for $LaFe_{11.5-x}Co_xSi_{1.5}$ compounds with $\mu_0 \Delta H$ of 1 T are presented in Figure 5. T_C shift to larger temperature and a decrease of ΔS_M^{max} are clearly observed as the Co content increases.

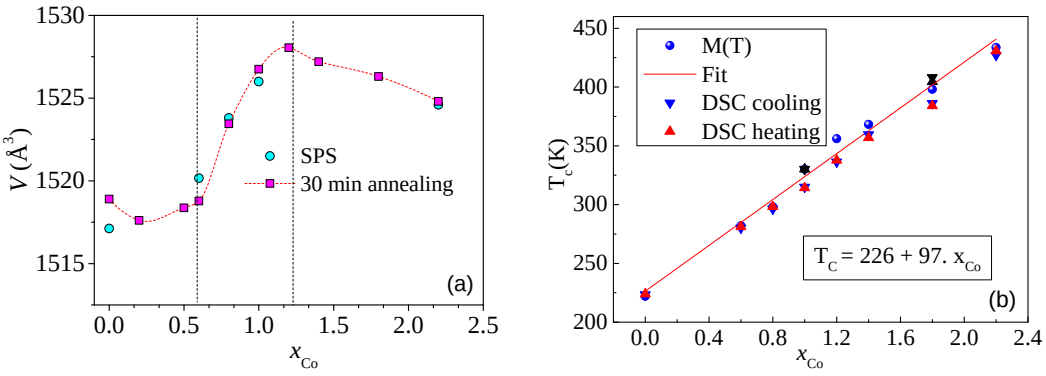

Figure 4. (**a**) Unit cell volume vs. Co content, (**b**) T_C vs. Co content, for $LaFe_{11.5-x}Co_xSi_{1.5}$ [52].

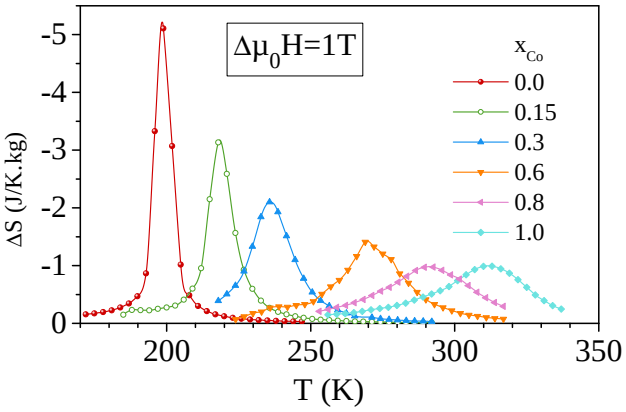

Figure 5. Magnetic ΔS_M variations for different x Co content for $LaFe_{11.5-x}Co_xSi_{1.5}$ [52].

The ^{57}Fe Mössbauer spectra that were collected at room temperature, for x = 0.8, 1, 1.2, and 2.2, have been refined with several ferromagnetic sextets for both inequivalent 8*b* and 96*i* iron sites. The obtained weighted average hyperfine field $< B_{HF} >$, together with T_C, versus x Co content, are shown in Figure 6. As the Co content becomes larger, an increase of the mean Fe local moment is observed. It is worth noticing that the Co substitution increases both T_C and the iron local moment.

Gebara et al. [53] have studied $LaFe_{11.8-x}Co_xSi_{1.2}$ alloys ($x = 0.52, 0.66, 0.8, 0.94, 1.08$) composites that were prepared by high energy ball milling showing the evolution of lattice constant, the Curie temperature, magnetic entropy change, and the evolution of the Fe Mössbauer spectra. Surprisingly, the magnetic entropy changes are not very sensitive to the Co content in their composites.

The substitution of Fe by the Z elements (Z = V, Cr, Ni, Cu) in the $La(Fe_{1-x}Z_x)_{11.4}Si_{1.6}$ system can lead to a strong influence on the electron concentration on the magnetic and magnetocaloric properties [54]. This is due to the properties of itinerant metamagnets that are very sensitive to the 3*d* electron density at the Fermi level. For this motivation, Pathak et al. [54] have studied the possibility of substituting Fe by other 3*d* metals (V, Cr, Ni, Cu).

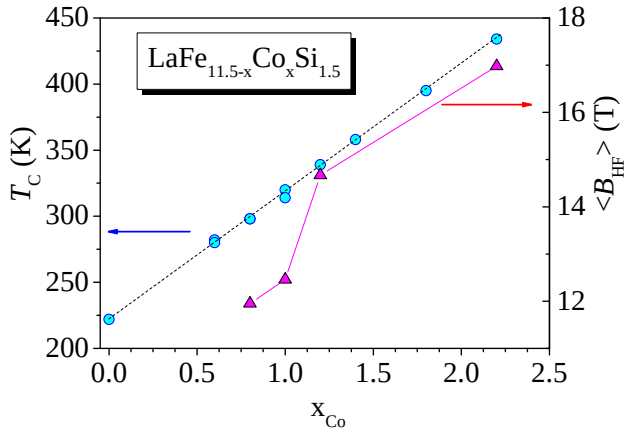

Figure 6. Evolution of the Curie temperature T_C and the weighted average hyperfine field $< B_{\mathrm{HF}} >$ versus x Co content [52].

For Z = V and at low Z substitution rates, in $La(Fe_{1-x}Z_x)_{11.4}Si_{1.6}$, a loss of the magnetocaloric effect and an increase in T_C are observed, $T_C = 211$ K for $x = 0$ increases up to 223 K for $x = 0.01$, and $\Delta S_{\mathrm{M}}^{\max}$ decreases from 15 to 8 J/kg.K. On the contrary, a substitution of Fe by Mn in $La(Fe_{1-x}Mn_x)_{11.7}Si_{1.3}$ [55] shows a decrease in T_C, as well as a decrease of $\Delta S_{\mathrm{M}}^{\max}$.

5. Effect of La Substitution in $La_{1-Z}R_z(Fe,Si)_{13}$

The substitution of La by another rare earth atom influences the structural and magnetic properties of the material. Anh et al. [56] performed a systematic study on the effect of Nd substitution on magnetocaloric effect in $La_{1-z}Nd_zFe_{11.44}Si_{1.56}$ ($z = 0 - 0.4$). They found a decrease of the unit cell parameter and $\Delta S_{\mathrm{M}}^{\max}$ with an increasing Nd content.

Fujita et al. [57,58] and Fujieda et al. [59,60] studied the effect of partial substitution of La in $La(Fe_{0.88}Si_{0.12})_{13}$ compound. Figure 7 (Left) shows that the unit cell parameter and T_C linearly decrease with Ce/Pr content; these results were mainly attributed to the magnetovolume effect [59,60].

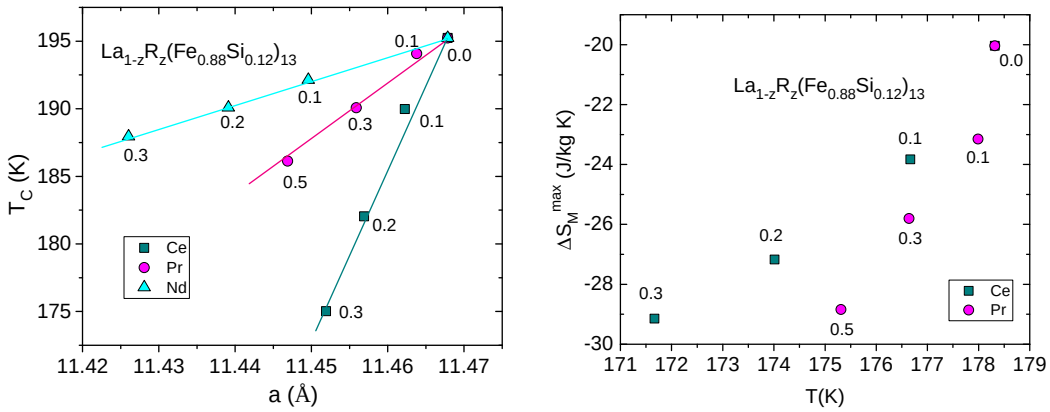

Figure 7. (**Left**) Evolution of T_C vs. unit cell parameter, (**Right**) $\Delta S_{\mathrm{M}}^{\max}$ vs. T_C, for $La_{1-z}R_z(Fe_{0.88}Si_{0.12})_{13}$ (R = Ce, Pr, Nd) [57–62].

In addition, $\Delta S_{\mathrm{M}}^{\max}$ increases with the substitution rate (Figure 8). We can see that the effect is more contrasted with Ce atoms, which can be tetravalent. In an alloy, its average valence is therefore greater than three and its average ionic radius is smaller than for other rare earths.

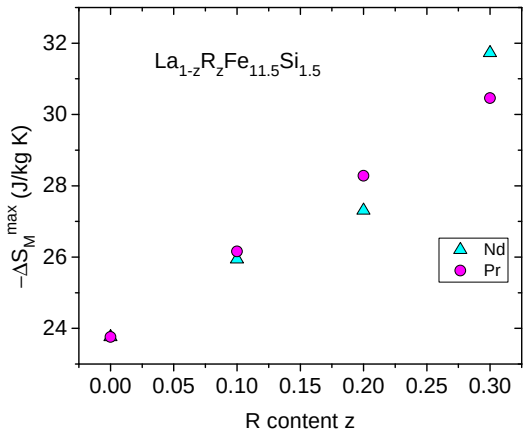

Figure 8. $\Delta S_{\mathrm{M}}^{\max}$ vs. R content z, for $La_{1-z}R_zFe_{11.5}Si_{1.5}$ (R = Nd, Pr) [61,62].

The effect of substituting La by another rare earth atom on the unit cell parameter, T_C, and MCE was also studied by Shen et al. [61,62] for (R = Ce, Pr, Nd) and by P. Gebara and J. Kovac [63,64] for (R = Dy, Ho).

The maximum value of $\Delta S_{\mathrm{M}}^{\max}$ was found to increase from 23.7 J/(kg.K) for $z = 0$ to 32.0 J/(kg.K) for $z = 0.3$ in $La_{1-z}Nd_zFe_{11.5}Si_{1.5}$, for a field change $\mu_0 \Delta H$ of 0-5 T, but this comes with a change of the hysteresis loss from 21.2 J/kg to 77.5 J/kg. Moreover, the relative cooling power (RCP) is enhanced by the partial substitution of Nd [61,62]. On the other hand, the substitution of La by Ho or Dy causes a decrease of magnetic entropy change [63,64].

6. Effect of Light Element Insertion in $La(FeSi)_{13}X$

6.1. Hydrogen Insertion

Fujieda et al. [65] and Fujita et al. [35] have shown that the insertion of hydrogen atoms (H) into $La(Fe_{0.88}Si_{0.12})_{13}$ significantly increases the Curie temperature, which increases linearly with the hydrogen content while maintaining the first order character of the transition. They have controlled the hydrogen concentration by changing both the annealing temperature and the hydrogen gas pressure. Fujieda et al. [65] adjusted T_C to around room temperature (278 K) by hydrogen absorption. Fujita et al. [35] showed that, due to the increase of T_0, temperature at which the IEM transition disappears, this phenomenon appears above the Curie temperature, Figure 9 (Right). The disappearance of the IEM transition reflects the suppression of the renormalization effect due to the cell volume expansion of the $La(Fe_{0.88}Si_{0.12})_{13}H_y$ compounds through magnetovolume effects.

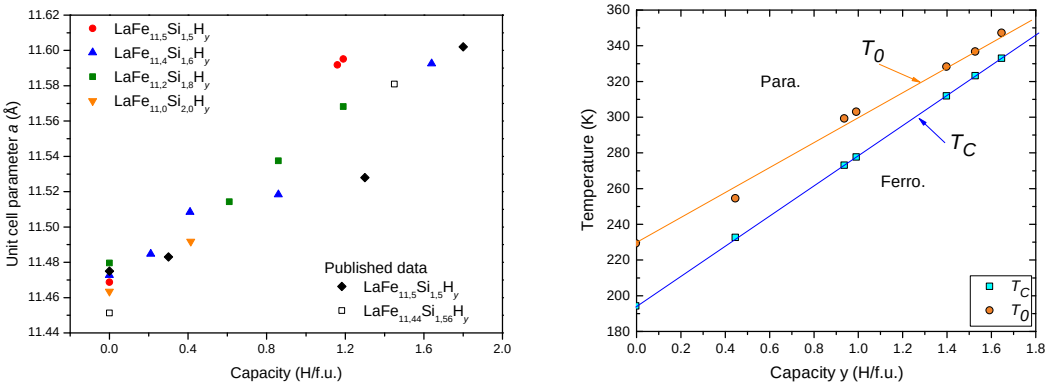

Figure 9. (**Left**) Unit cell parameter a vs. hydrogen content [66,67]. (**Right**) Magnetic phase diagram of $LaFe_{11.44}Si_{1.56}H_y$. The IEM transition occurs between T_0 (the temperature at which the IEM transition disappears) and T_C [35].

Phejar et al. [68] found that the unit cell parameter a increases linearly with hydrogen content, independent of the composition of the parent compound; this result is in agreement with previous results [66,67] (Figure 9-Left). In order to follow the evolution of the crystallographic and magnetic parameters as a function of the temperature, they have performed NPD experiments between 1.5 and 300 K. In order to have a smaller incoherent background and, therefore, a better signal/noise ratio, the hydrogen is replaced by deuterium (D). The $La(Fe_{0.88}Si_{0.12})_{13}D_{0.7}$ compound exhibited a magnetostrictive effect around T_C, resulting in a contraction of the cell parameter at the transition, which is the result of the IEM transition, as shown in Figure 10 (left). The cell parameter of the α-(Fe,Si) inclusions increases, as expected, from a thermal expansion behavior without anomaly at T_C. A different behavior has been found by Gebara et al. [69], where an anomalous behavior of α-Fe impurity cell parameter was observed at T_C in $La(Fe,Si)_{13}$ compounds with La substituted by Ce, Pr, Ho, or Fe by Mn. This means that micro-strains are negligible in the deuteride. Figure 10 (right) shows the magnetic moments of Fe{96*i*} and Fe{8*b*} atoms in the $LaFe_{11.5}Si_{1.5}D_{0.7}$ compound.

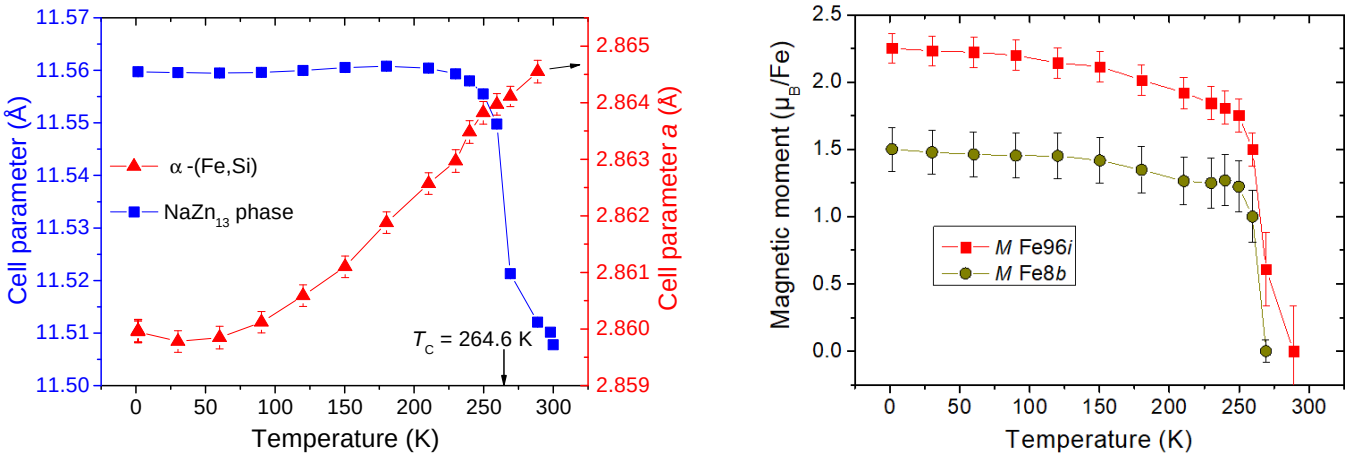

Figure 10. (**Left**) Evolution of the deuteride $LaFe_{11.5}Si_{1.5}D_{0.7}$ cell parameter versus temperature derived from neutron diffraction. (**Right**) Magnetic moments of Fe atoms versus temperature, in the 96*i* and 8*b* crystallographic sites [68].

Neutron powder diffraction (NDP) experiments have been performed to solve the structure and localize the interstitial site In order to remove ambiguity concerning the interstitial occupied by hydrogen (deuterium) or carbon (24*d* or 48*f* site) [68]. Paul-Boncour et al. [68,70] have refined the NDP patterns while using the Rietveld method and have found that the interstitial D(H) was located on the 48*f* site (Figure 11); this result is in perfect agreement with previous work [67].

Mandal et al. [71] showed that they have succeeded in tuning the Curie temperature from 199 to 346 K, with the hydrogen content without changing significantly ΔS_M^{max} value.

Figure 12 (Left) shows the evolution of the Curie temperature for materials in which hydrogen has been inserted as a function of the insertion rate y_H taken from different works [35,68,71,72]. Figure 12 (Right) shows the evolution of ΔS_M^{max} versus the insertion rate y_H for $LaFe_{13-x}Si_xH_y$ [35,68,71]. According to this figure, it can be noticed that, for the Si content $1.3 \leq x \leq 1.6$, we obtain a first-order magnetic transition, which results in a larger ΔS_M^{max} than for the compositions $x \geq 1.8$, which represent a second-order magnetic transition. Moreover, for $x = 1.4$ and 1.6, ΔS_M^{max} is almost constant for the different hydrogen insertion rates y_H.

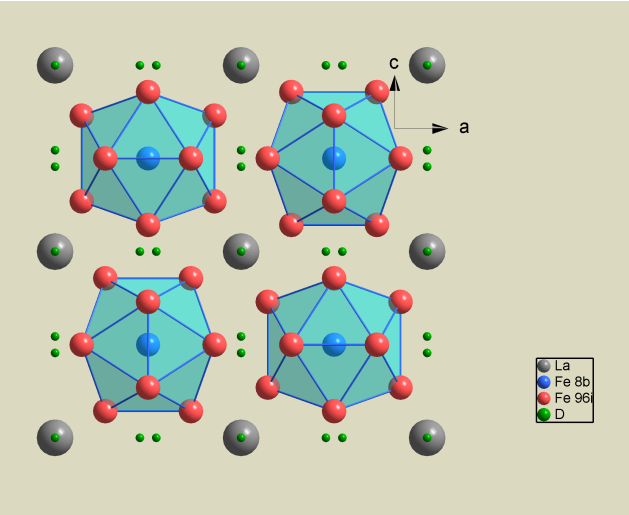

Figure 11. The unit cell of $LaFe_{11.5}Si_{1.5}D_{0.7}$ projected along the (a, c) plane.

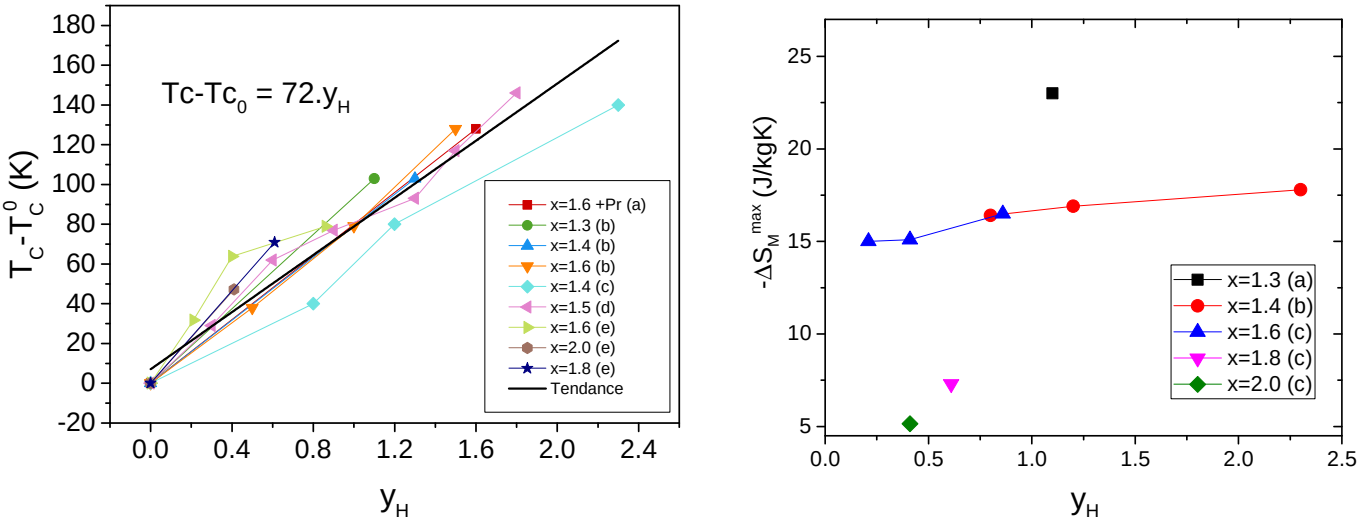

Figure 12. (**Left**) Evolution of the Curie temperature for materials in which hydrogen has been inserted vs. the insertion rate y_H (a) [72], (b) [35], (c) [71], (d) [68], and (e) [70]. (**Right**) ΔS_M^{max} vs. the insertion rate y_H for $LaFe_{13-x}Si_xH_y$ (a) [35], (b) [71], and (c) [68].

6.2. Carbon Insertion

Another possibility for increasing unit cell parameters and, thus, the Curie temperature of the material by magneto-volumic effect is the insertion of carbon atoms into the interstitial sites of the structure. This carbon insertion induces a decrease in ΔS_M. The insertion of carbon in the material changes the electronic state and, thus, the magnetic properties of the material. The decrease of ΔS_M as a function of T_C is of the same order as that obtained by the substitution of iron by cobalt: a decrease in entropy of 19 J/kg.K for an increase in T_C of 100 K. Thus, it seems that, in this case, the transition also goes from first order to second order.

Li et al. [73] studied the insertion of carbon influences the phase formation, T_C, and magnetic entropy change of $LaFe_{11.7}Si_{1.3}$. The unit cell parameter a increases with C content, T_C increases from 194 to 225 K, and ΔS_M was equal to 27.5 $J.kg^{-1}K^{-1}$.

Phejar et al. [68] studied the effect of the carbonation of $LaFe_{13-x}Si_x$ compounds. $LaFe_{11.5}Si_{1.5}C_{0.7}$ compound displays a magnetostrictive effect around T_C and a classical thermal expansion for the α-(Fe,Si) impurities as for the deuteride, as shown in

Figure 13 (left). Figure 13 (right) shows the evolution of the magnetic moments versus the temperature. The magnetic moment decrease is not as abrupt when compared to the hydrides, which is due to a weakening of the first order transition.

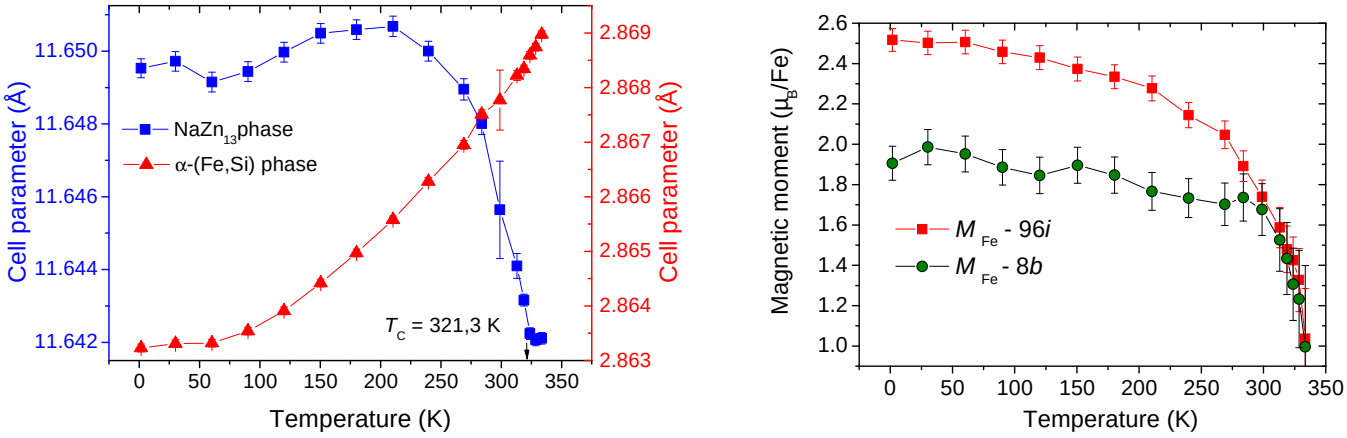

Figure 13. Unit cell parameter *a* vs. temperature for $LaFe_{11.5}Si_{1.5}C_{0.7}$ (**left**). Magnetic moments of Fe atoms vs. temperature, in the 96*i* and 8*b* crystallographic sites (**right**). The results are obtained from neutron diffraction [68].

7. Combination of Substitution and Light Element Insertion

Hydrogen insertion in $La(Fe_{1-x}Si_x)_{13}$ compounds allow for maintaining a large magnetic entropy variation with T_C at room temperature (RT). However, several studies have shown that, for H composition lower than 1.5 H/f.u. and with T_C close to room temperature, there is a splitting into two hydride phases with low and high H concentrations after few hours or weeks at RT [55,74,75]. The sample is no more homogeneous and the magnetic entropy variation is split in two peaks. In order to avoid this segregation, it is safer to prepare saturated hydrides, but their Curie temperature is around 330–340 K. This temperature can be reduced to RT by partial Mn for Fe substitution for a fully hydrogenated hydride. In this case, the hydride remains stable without desorption or segregation versus time or upon magnetic cycles, despite T_C being near RT. A systematic study on the influence of Mn for Fe substitution [76] has revealed that it is possible to vary T_C between 260 and 350 K ($0.1 \leq x_{Mn} \leq 0.4$ Mn/f.u; Si concentrations: 1.2 and 1.4 Si/f.u. and $1.77 \leq y_H \leq 1.97$ H/f.u.). The drawback is a significant reduction of the ΔS_M and ΔT_{ad} values as the Mn content increases significantly [77], but this Mn substitution remains interesting to vary T_C in a narrow temperature range, as, in this case, the reduction of ΔS_M is limited [78].

Another alternative is to partially substitute La by Ce [79], as, beside the reduction of T_C, there is an increase of the MCE effect versus the rate of Ce for La substitution. However, it was found that, in this case, the hydrogenation significantly reduces the MCE effect as compared to that of the parent alloys, which is less beneficial than expected. The influence of Ce substitution for carbides was also investigated, but, despite the larger magneto-volume effect of C versus H insertion, the reduction of ΔS_M was more pronounced [50]. Hai et al. [80,81] studied the influence of both C and H insertion on Ce substituted alloys on the hydrogenation kinetic by in-situ neutron diffraction. The preferential insertion of C in 24 *d* sites introduces a cell distortion and modifies some specific Fe-Fe distances. The presence of C is found to influence the H insertion and to slow down the hydrogenation kinetic. The presence of Ce substituted to La also modifies the kinetic of reaction due to its smaller atomic radius.

Further studies have been undertaken to combine both Ce for La and Mn for Fe substitution with hydrogen insertion [27,82,83]. An adjustment of the rate of both Ce and Mn in $La_{0.9}Ce_{0.1}Fe_{11.7-x}Mn_xSi_{1.3}$ hydrides allows for maintaining a significant MCE effect near RT. The influence of the bonding with epoxy [27,82] was found to improve the

mechanical properties and slightly reduce the MCE effect. High hydrogen pressure sintering on $La_{0.9}Ce_{0.1}Fe_{11.7-x}Mn_xSi_{1.3}$ hydrides [83] showed a beneficial effect for a pressure of 40 MPa. However, an applied pressure of 50 MPa induced the precipitation of α-Fe reducing the MCE effect.

Beside these works, the influence of Co insertion on the magnetocaloric properties of hydrides has been investigated [70]. The aim was not to maintain T_C near RT, but rather to increase it for heat pump applications above room temperature. T_C is found to increase linearly versus Co content and H concentration for $LaFe_{10.5-x}Co_xSi_{1.5}H_y$ compounds (Figure 14 (Left)), but the dT_C/dy slope changes versus Co concentration. T_C can be expressed as a function of x and y while taking a negative mixing term into account:

$$T_C(x, y) = 210 + 100 \cdot x + 83 \cdot y - 18 \cdot x \cdot y$$

For $x = 1$ and $y = 1.5$, $T_C = 400$ K, whereas it would have been 450 K without the negative exchange term.

The Co substitution induces a reduction of the magnetic entropy variation, whereas it remain almost constant before and after hydrogenation, as shown for $x_{Co} = 0.8$ and $y = 1.4$ (Figure 14 (Right)).

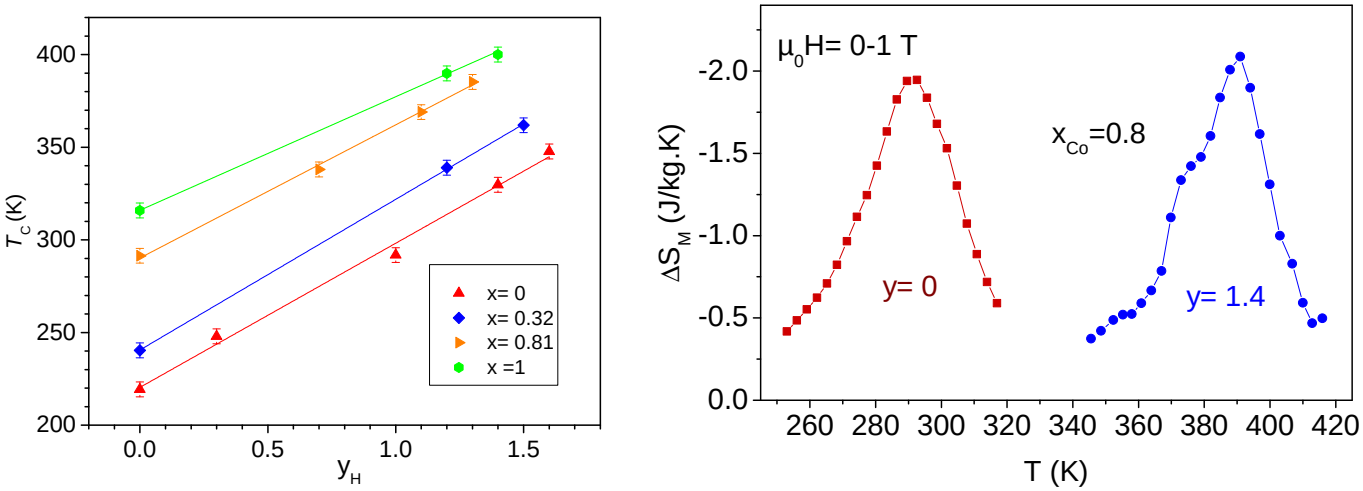

Figure 14. (**Left**) Evolution of T_C versus H concentration for different Co rates, (**Right**) Comparison of ΔS_M for $LaFe_{9.7}Co_{0.8}Si_{1.5}H_y$ ($y = 0$ and 1.4) and a field variation 0-1 T.

8. Implementation in Active Magnetic Regenerators

The optimization of the chemical composition by the substitution or/and light element insertion in $La(Fe,Si)_{13}$ compounds has been reviewed in previous part. But magnetic refrigeration requires also the use of an active magnetic regenerator (AMR) to increase the temperature span (ΔT_{span}) by generating a temperature gradient between the hot and cold sources [84]. Many prototypes have been tested while using Gd or its alloys as reference refrigerants in AMR [85]. Although Gd offer many advantages (stability, easy to machine, large ΔT_{ad}, the absence of thermal hysteresis, large thermal conductivity), its elevated cost and limited global reserve constitutes a serious drawback for a broad public application. Therefore, it is necessary to test and optimize other promising magnetocaloric material, such as $La(Fe,Si)_{13}$ in AMR. The performances of different regenerators using Gd and $La(Fe,Co,Si)_{13}$ material have been compared and discussed in [86–89]. In all of these prototypes, the AMR were fixed and the magnetic field mobile (rotation of permanent magnets arranged in Halbach cylinder or reciprocating movement). One of the best geometries to favor heat exchange is thin parallel plates (0.25–1 mm) that are separated by a small gap [87,90]. Compared to Gd, which presents broad ΔS_M and ΔT_{ad} peaks, $La(Fe,Co,Si)_{13}$ compounds display higher but narrower peaks due to their first order

transition. In addition, due to its smaller specific heat, Gd has a two time larger ΔT_{ad} than La(Fe,Co,Si)$_{13}$ for a field variation around 1 T. To expand the ΔT_{span}, the use of a composite or several plates of La(Fe,Co,Si)$_{13}$ compounds with different T_C, obtained by varying the Co content, have been therefore tested. Thin plates prepared by TDR method and purchased by Vacuumschmelze GmbH and Co were used in several prototypes [86–88]. Other tests were performed with an epoxy-bonded plates [89]. Better performances were obtained while using regenerators with at least four different compositions that were arranged to optimize the thermal gradient, as compared to plates with only one or two different compositions.

Balli et al. [86] built a prototype with two AMRs that are alternatively magnetized and demagnetized in order to reduce the magnetic forces acting on the magnetic refrigerant. The applied magnetic field is parallel to the plates to limit the demagnetization field which is corrected. Working with two AMR, one with Gd and the other with a La(Fe,Co,Si)$_{13}$ composite, they obtained a comparable maximum ΔT_{span} of 14 and 16 K for LaFeSi-based and Gd AMR respectively. They have tested the corrosion behavior of La-Fe-Co-Si compounds in different solutions of water with an additional corrosion inhibitor and a silicon oil. The best resistance to corrosion was obtained with 3% of noxal anti-oxidant. Because water has a larger specific heat (C_p = 4.2 J/g K) than Si oil (C_p = 1.6 J/g K), it is more favorable as fluid heat transfer. The study of the corrosion of Gd and La(Fe,Co,Si)$_{13}$ in various heat conducting fluids is detailed in Forchelet et al. [91].

Legait et al. [88] compared the performance of Gd, a manganite oxide ($Pr_{0.65}Sr_{0.35}MnO_3$) and La(Fe,Co)$_{13-x}$Si$_x$ compounds under a wide range of fluidic and magnetic operating conditions. Their devices do not use a thermal exchanger, therefore it only provides non-load temperature spans. They have followed the influence of non-dimensional numbers (utilization ratio U and volume ratio V^*) and physical properties, such as thermal conductivity. They observed that each regenerator is most efficient over a specific domain of utilization. A material with low thermal conductivity (manganite) is more efficient at low frequency, whereas the materials with large thermal conductivity are better at a high frequency.

Tusek et al. [87] have tested their AMR with a device that is equipped with a reciprocating magnet and a heat exchanger to investigate the cooling load under different ΔT_{span}. They have observed that the maximum ΔT_{span} varies versus the utilization factor U and the operating frequency P. It is larger for LaFeSi-based AMR when compared to Gd at low U values (moderate ΔT_{span}), whereas that of Gd increases for larger U values. The maximum ΔT_{span} also depends on the hot side temperature and it is maximum at 35 °C for Gd, 27 °C for a two-layered, and 43 °C for a seven-layered La(Fe,Co,Si)$_{13}$ AMR

AMR was also prepared with epoxy-bonded plates that were constituted of a composite of La(Fe,Co)$_{13-x}$Si$_x$ powder in a polymer matrix pressed into thin plates [89]. This AMR yields smaller ΔT_{span} than with sintered plates, but it has very good mechanical properties, as it remains stable without significant changes over 90,000 cycles. Because the AMR was constituted with two-layered plates (two different T_C), further improvements can be expected by preparing a AMR with four-layered plates. Beside these experimental results, numerical investigations have been performed through a two-dimensional (2D) model of an AMR refrigerator for various magnetocaloric materials [92,93]. The best performance in terms of temperature spans and coefficient of performance (COP) were obtained for Gd, $Gd_5Si_2Ge_2$, La(Fe,Mn,Si)$_{13}$H$_y$, and La(Fe,Co,Si)$_{13}$ compounds as compared to MnFe(P,As) and manganite oxide.

The thickness of the plates as well as the spacing between the plates, the T_C distribution, the intensity of the magnetic field, and the operating frequencies are among the important parameters for optimizing in order to obtain the best cooling performances. Therefore, the properties of AMR with La(Fe,Co,Si)$_{13}$ material should be optimized to reach as good AMR performances as Gd. These materials remain very promising for magnetic refrigeration near room temperature application due to their many advantages in term of cost and global reserve.

9. Conclusions

In this review, we have presented the main works dealing with the magnetocaloric effect of $LaFe_{13-x}Si_x$. The different methods of synthesis and shaping were presented and compared. The influence of both chemical substitution of La, Fe, and Si by other elements, as well as the insertion of light elements (H, C), were presented to show the advantages and disadvantages of each solutions. Fe for Co substitution or H insertion are considered to be the most efficient way to use these materials as refrigerant near room temperature. A combination of metal substitution and light element insertion is another alternative to adjust their working conditions. $La(Fe,Si)_{13}$ type compounds have been implemented in active magnetic regenerators and their performance in magnetic refrigerator prototype when compared with that of Gd.

Author Contributions: Conceptualization, V.P.-B. and L.B.; methodology, V.P.-B. and L.B.; validation, V.P.-B. and L.B.; formal analysis, V.P.-B. and L.B.; investigation, V.P.-B. and L.B.; data curation, V.P.-B. and L.B.; writing—original draft preparation, V.P.-B. and L.B.; writing—review and editing, V.P.-B. and L.B.; visualization, V.P.-B. and L.B. All authors have read and agreed to the published version of the manuscript.

Funding: This research received no external funding.

Institutional Review Board Statement: Not applicable.

Informed Consent Statement: Not applicable.

Data Availability Statement: Data available on request due to restrictions eg privacy or ethical.

Acknowledgments: The work of our group was done in the frame of the PhD thesis of M. Phejar and A. Patissier, as well as the master work of K. Nakouri.

Conflicts of Interest: The authors declare no conflict of interest.

Abbreviations

AMR	Active Magnetic Regenerator
COP	Coefficient of Performance
DSC	Differential Scanning Calorimetry
FM	Ferromagnetic
IEM	Itinerant Electron Metamagnetic
MCE	Magnetocaloric effect
NPD	Neutron Powder Diffraction
PM	Paramagnetic
RT	Room Temperature
SPS	Spark Plasma Sintering
T_C	Curie Temperature
TDR	Thermal Decomposition and Recombination
RCP	Relative Cooling Power
ZFC-FC	Zero Field Cooled - Field Cooled

References

1. Kitanovski, A.; Tusek, J.; Tomc, U.; Plaznik, U.; Ozbolt, M.; Poredos, A. *Magnetocaloric Energy Conversion, From Theory to Applications*; Springer International Publishing: Cham, Switzerland, 2015.
2. Aprea, C.; Greco, A.; Maiorino, A.; Masselli, C. The employment of caloric-effect materials for solid-state heat pumping. *Int. J. Refrig.* **2020**, *109*, 1–11. [CrossRef]
3. Nikitin, S.A.; Myalikgulyev, G.; Tishin, A.M.; Annaorazov, M.P.; Asatryan, K.A.; Tyurin, A.L. The magnetocaloric effect in $Fe_{49}Rh_{51}$ compound. *Phys. Lett. A* **1990**, *148*, 363–366. [CrossRef]
4. Pecharsky, V.K.; Gschneidner, K.A. Giant Magnetocaloric Effect in $Gd_5(Si_2Ge_2)$. *Phys. Rev. Lett.* **1997**, *78*, 4494. [CrossRef]
5. Wada, H.; Tomekawa, S.; Shiga, M. Magnetocaloric properties of a first-order magnetic transition system $ErCo_2$. *Cryogenics* **1999**, *39*, 915–919. [CrossRef]

6. Wada, H.; Tanabe, Y. Giant magnetocaloric effect of $MnAs_{1-x}Sb_x$. *Appl. Phys. Lett.* **2001**, *79*, 3302–3304. [CrossRef]
7. Valiev, E.; Gimaev, R.; Zverev, V.; Kamilov, K.; Pyatakov, A.; Kovalev, B.; Tishin, A. Application of the exchange-striction model for the calculation of the FeRh alloys magnetic properties. *Intermetallics* **2019**, *108*, 81–86. [CrossRef]
8. Gimaev, R.R.; Vaulin, A.A.; Gubkin, A.F.; Zverev, V.I. Peculiarities of Magnetic and Magnetocaloric Properties of Fe-Rh Alloys in the Range of Antiferromagnet-Ferromagnet Transition. *Phys. Metals Metallogr.* **2020**, *121*, 823–850. [CrossRef]
9. Sanchez-Valdas, C.F.; Gimaev, R.R.; Lopez-Cruz, M.; Llamazares, J.L.S.; Zvereve, V.I.; Tishin, A.M.; Carvalho, A.M.G.; Aguiar, D.J.M.; Mudryk, Y.; Pecharsky, V.K. The effect of cooling rate on magnetothermal properties of $Fe_{49}Rh_{51}$. *J. Magn. Magn. Mater.* **2020**, *498*, 166130. [CrossRef]
10. Zarkevich, N.A.; Zverev, V.I. Viable Materials with a Giant Magnetocaloric Effect. *Crystals* **2020**, *10*, 815. [CrossRef]
11. Zverev, V.I.; Gimaev, R.R.; Miyanaga, T.; Vaulin, A.A.; Gubkin, A.F.; Kovalev, B.B.; dos Santos, A.M.; Lovell, E.; Cohen, L.F.; Zarkevich, N.A. Peculiarities of the phase transformation dynamics in bulk FeRh based alloys from magnetic and structural measurements. *J. Magn. Magn. Mater.* **2021**, *522*, 167560. [CrossRef]
12. Raghavan, V. Fe-La-Si (Iron-Lanthanum-Silicon). *J. Phase Equilib.* **2001**, *22*, 158. [CrossRef]
13. Niitsu, K.; Kainuma, R. Phase equilibria in the Fe-La-Si ternary system. *Intermetallics* **2012**, *20*, 160–169. [CrossRef]
14. Liu, X.D.; Liu, X.B.; Altounian, Z.; Tu, G.H. Microstructures of $(Fe_{0.88}Co_{0.12})_{82}La_7Si_{11}$ prepared by arc-melting/melt spinning and subsequent annealing. *Appl. Phys. A Mater.* **2006**, *82*, 339–343. [CrossRef]
15. Fujita, A.; Koiwai, S.; Fujieda, S.; Fukamichi, K.; Kobayashi, T.; Tsuji, H.; Kaji, S.; Saito, A.T. Magnetocaloric effect in spherical $La(Fe_xSi_{1-x})_{13}$ and their hydrides for active magnetic regenerator-type refrigerator. *J. Appl. Phys.* **2009**, *105*, 07A936. [CrossRef]
16. Fujita, A.; Yako, H. Stability of metallic, magnetic and electronic states in $NaZn_{13}$-type $La(Fe_xSi_{1-x})_{13}$ magnetocaloric compounds. *Scripta Mater.* **2012**, *67*, 578–583. [CrossRef]
17. Gebara, P.; Pawlik, P.; Skorvanek, I.; Bednarcik, J.; Marcin, J.; Michalik, S.; Donges, J.; Wyslocki, J.J.; Michalski, B. Effect of Al content on the order of phase transition and magnetic entropy change in $LaFe_{11}Co_{0.8}(Si_{1-x}Al_x)_{1.2}$ alloys. *J. Magn. Magn. Mater.* **2014**, *372*, 201–207. [CrossRef]
18. Liu, T.; Chen, Y.G.; Tang, Y.B.; Xiao, S.F.; Zhang, E.Y.; Wang, J.W. Structure and magnetic properties of shortly high temperature annealing $LaFe_{11.6}Si_{1.4}$ compound. *J. Alloys Compd.* **2009**, *475*, 672–675. [CrossRef]
19. Gutfleisch, O.; Yan, A.; Muller, K.H. Large magnetocaloric effect in melt-spun $LaFe_{13-x}Si_x$. *J. Appl. Phys.* **2005**, *97*, 10M305. [CrossRef]
20. Liu, X.B.; Liu, X.D.; Altounian, Z.; Tu, G.H. Phase formation and structure in rapidly quenched $La(Fe_{0.88}Co_{0.12})_{13-x}Si_x$ alloys. *J. Alloys Compd.* **2005**, *397*, 120–125. [CrossRef]
21. Liu, X.B.; Liu, X.D.; Altounian, Z. Phase formation and magnetocaloric effect in rapidly quenched $La(Fe_{1-x}Co_x)_{11.4}Si_{1.6}$. *J. Appl. Phys.* **2005**, *98*, 113904. [CrossRef]
22. Yan, A. Structure and magnetocaloric effect in melt-spun La $(Fe,Si)_{13}$ and MnFePGe compounds. *Rare Met.* **2006**, *25*, 544–549. [CrossRef]
23. Lyubina, J.; Gutfleisch, O.; Kuzmin, M.D.; Richter, M. $La(Fe,Si)_{13}$-based magnetic refrigerants obtained by novel processing routes. *J. Magn. Magn. Mater.* **2008**, *320*, 2252–2258. [CrossRef]
24. Dong, J.D.; Yan, A.R.; Liu, J. Microstructure and magnetocaloric properties of melt-extracted La-Fe-Si microwires. *J. Magn. Magn. Mater.* **2014**, *357*, 73–76. [CrossRef]
25. Liu, J.; Zhang, P.N.; Dai, F.P.; Yan, A.R. A new approach to prepare spherical La-Fe-Si-Co magnetocaloric refrigerant particles. *Scripta Mater.* **2013**, *69*, 485–488. [CrossRef]
26. Fujita, A.; Nakayama, Y.; Kano, M.; Matsunami, D. Improvement of low-field magnetic entropy change by increasing Fe concentration in solid-state reactive sintered $La(Fe_xSi_{1-x})_{13}$. *J. Alloys Compd.* **2014**, *601*, 158–161. [CrossRef]
27. Mayer, C.; Dubrez, A.; Pierronnet, M.; Vikner, P. Towards the large scale production of $(La_{1-z}Ce_z)(Fe_{1-x-y}Mn_ySi_x)_{13}$H-n products for room temperature refrigeration. *Phys. Status Solidi C.* **2014**, *11*, 1059–1063. [CrossRef]
28. Katter, M.; Zellmann, V.; Reppel, G.W.; Uestuener, K. Magnetocaloric Properties of $La(Fe,Co,Si)_{13}$ Bulk Material Prepared by Powder Metallurgy. *IEEE Trans. Magn.* **2008**, *44*, 3044–3047. [CrossRef]
29. Katter, M.; Zellmann, V.; Barcza, A. Sintering behavior and thermally induced decomposition and recomposition processe of $LaFe_{13-x-y}Co_xSi_y$. In Proceedings of the Fourth IIF-IIR International Conference on Magnetic Refrigeration at Room Temperature, Thermag IV, IIF-IIR, Baotou, China, 23–27 August 2010.
30. Phejar, M.; Paul-Boncour, V.; Bessais, L. Structural and magnetic properties of magnetocaloric $LaFe_{13-x}Si_x$ compounds synthesized by high energy ball-milling. *Intermetallics* **2010**, *18*, 2301–2307. [CrossRef]
31. Patissier, A.; Paul-Boncour, V. Fast synthesis of $LaFe_{13-x}Si_x$ magnetocaloric compounds by reactive Spark Plasma Sintering. *J. Alloys Compd.* **2015**, *645*, 143–150. [CrossRef]
32. Moore, J.D.; Klemm, D.; Lindackers, D.; Grasemann, S.; Trager, R.; Eckert, J.; Lober, L.; Scudino, S.; Katter, M.; Barcza, A.; et al. Selective laser melting of $La(Fe,Co,Si)_{13}$ geometries for magnetic refrigeration. *J. Appl. Phys.* **2013**, *114*, 043907. [CrossRef]
33. Paul-Boncour, V.; Pattisier, A.; Nakouri, K.; Bessais, L. Magnetocaloric compounds prepared by reactive spark plasma sintering. In Proceedings of the 7th International Conference on Caloric Cooling (Thermag VII), Turin, Italy, 11–14 September 2016.
34. Niitsu, K.; Fujieda, S.; Fujita, A.; Kainuma, R. Microstructure and magnetic properties of as-quenched cubic and tetragonal $La(Fe_{1-x}Si_x)_{13}$ compounds. *J. Alloys Compd.* **2013**, *578*, 220–227. [CrossRef]

35. Fujita, A.; Fujieda, S.; Hasegawa, Y.; Fukamichi, K. Itinerant-electron metamagnetic transition and large magnetocaloric effects in $La(Fe_xSi_{1-x})_{13}$ compounds and their hydrides. *Phys. Rev. B* **2003**, *67*, 104416. [CrossRef]
36. Moore, D.; Morrison, K.; Sandeman, K.G.; Katter, M.; Cohen, L.F. Reducing extrinsic hysteresis in first-order $La(Fe,Co,Si)_{13}$ magnetocaloric systems. *Appl. Phys. Lett.* **2009**, *95*, 252504. [CrossRef]
37. Yako, H.; Fujieda, S.; Fujita, A.; Fukamichi, K. Influence of Demagnetization Effect on the Kinetics of the Itinerant Electron Metamagnetic Transition in Magnetic Refrigerant $La(Fe_{0.88}Si_{0.12})_{13}$. *IEEE Trans. Magn.* **2011**, *47*, 2482–2485. [CrossRef]
38. Lovell, E.; Pereira, A.M.; Caplin, A.D.; Lyubina, J.; Cohen, L.F. Dynamics of the First-Order Metamagnetic Transition in Magnetocaloric $La(Fe,Si)_{13}$: Reducing Hysteresis. *Adv. Energy Mater.* **2015**, *5*, 1401639. [CrossRef]
39. Cohen, L.F. Contributions to Hysteresis in Magnetocaloric Materials. *Phys. Status Solidi (b)* **2018**, *255*, 1700317.
40. Lovell, E.; Morrison, K.; Pereira, A.M.; Caplin, A.D.; Gutfleisch, O.; Cohen, L.F. Scanning Hall Probe Imaging of $LaFe_{13-x}Si_x$. *Adv. Sci. Tech.* **2014**, *93*, 219–224. [CrossRef]
41. Ido, H.; Sohn, J.C.; Pourarian, F.; Cheng, S.F.; Wallace, W.E. Magnetic properties of $LaCo_{13}$-based systems. *J. Appl. Phys.* **1990**, *67*, 4978. [CrossRef]
42. Hu, F.X.; Shen, B.G.; Sun, J.R.; Wang, G.J.; Cheng, Z.H. Very large magnetic entropy change near room temperature in $LaFe_{11.2}Co_{0.7}Si_{1.1}$. *Appl. Phys. Lett.* **2002**, *80*, 826–828. [CrossRef]
43. Bjork, R.; Bahl, C.R.H.; Katter, M. Magnetocaloric properties of $LaFe_{13-x-y}Co_xSi_y$ and commercial grade Gd. *J. Magn. Magn. Mater.* **2010**, *322*, 3882–3888. [CrossRef]
44. Hansen, B.R.; Kuhn, L.T.; Bahl, C.R.H.; Lundberg, M.; Ancona-Torres, C.; Katter, M. Properties of magnetocaloric $La(Fe,Co,Si)_{13}$ produced by powder metallurgy. *J. Magn. Magn. Mater.* **2010**, *322*, 3447–3454. [CrossRef]
45. Hu, F.X.; Qian, X.L.; Sun, J.R.; Wang, G.J.; Zhang, X.X.; Cheng, Z.H.; Shen, B.G. Magnetic entropy change and its temperature variation in compounds $La(Fe_{1-x}Co_x)_{11.2}Si_{1.8}$. *J. Appl. Phys.* **2002**, *92*, 3620–3623. [CrossRef]
46. Balli, M.; Fruchart, D.; Sari, O.; Gignoux, D.; Huang, J.H.; Hu, J.; Egolf, P.W. Direct measurement of the magnetocaloric effect on $La(Fe_{13-x-y}Co_y)Si_x$. *J. Appl. Phys.* **2009**, *106*, 023902. [CrossRef]
47. Ilyn, M.; Tishin, A.; Hu, F.; Gao, J.; Sun, J.; Shen, B. Magnetocaloric properties of the $LaFe_{11.7}Si_{1.3}$ and $LaFe_{11.2}Co_{0.7}Si_{1.1}$ systems. *J. Magn. Magn. Mater.* **2005**, *290*, 712. [CrossRef]
48. Yan, A.; Muller, K.H.; Gutfleish, O. Magnetocaloric properties of the $LaFe_{11.7}Si_{1.3}$ and $LaFe_{11.2}Co_{0.7}Si_{1.1}$ systems. *J. Alloys Compd.* **2008**, *450*, 18. [CrossRef]
49. Dong, Q.Y.; Zhang, H.W.; Zhao, T.Y.; Sun, J.R.; Shen, B.G. Realization of a small hysteresis loss and a large magnetic entropy change in $NaZn_{13}$-type La-Fe-Si compound. *Solid State Commun.* **2008**, *147*, 266–270. [CrossRef]
50. Zhang, H.; Shen, J.; Xu, Z.Y.; Zheng, X.Q.; Hu, F.X.; Sun, J.R.; Shen, B.G. Simultaneous enhancements of Curie temperature and magnetocaloric effects in the $La_{1-x}Ce_xFe_{11.5}Si_{1.5}C_y$ compounds. *J. Magn. Magn. Mater.* **2013**, *324*, 484–487. [CrossRef]
51. Hu, F.X.; Gao, J.; Qian, X.L.; Ilyn, M.; Tishin, A.M.; Sun, J.R.; Shen, B.G. Magnetocaloric effect in itinerant electron metamagnetic systems $La(Fe_{1-x}Co_x)_{11.9}Si_{1.1}$. *J. Appl. Phys.* **2005**, *97*, 10M303. [CrossRef]
52. Paul-Boncour, V.; Nakouri, K.; Pattisier, A.; Bessais, L. Fast synthesis and magnetocaloric properties of La(Fe, Co, Si)$_{13}$ compounds and their hydrides. In Proceedings of the 8th International Conference on Caloric Cooling (Thermag VIII), Darmstadt, Germany, 16–20 September 2018; pp. 593–598.
53. Gebara, P.; Pawlik, P. Broadening of temperature working range inmagnetocaloric $La(Fe,Co,Si)_{13}$- based multicomposite. *J. Magn. Magn. Mater.* **2017**, *442*, 145–151. [CrossRef]
54. Pathak, A.K.; Basnyat, P.; Dubenko, I.; Stadler, S.; Ali, N. Influence of the small substitution of Z=Ni, Cu, Cr, V for Fe on the magnetic, magnetocaloric, and magnetoelastic properties of $LaFe_{11.4}Si_{1.6}$. *J. Magn. Magn. Mater.* **2010**, *322*, 692–697. [CrossRef]
55. Barcza, A.; Katter, M.; Zellmann, V.; Russek, S.; Jacobs, S.; Zimm, C. Stability and Magnetocaloric Properties of Sintered $La(Fe,Mn,Si)_{13}H_z$ Alloys. *IEEE Trans. Magn.* **2011**, *47*, 3391–3394. [CrossRef]
56. Anh, D.T.K.; Thuy, N.P.; Duc, N.H.; Nhien, T.T.; Nong, N.V. Magnetism and magnetocaloric effect in $La_{1-y}Nd_y(Fe_{0.88}Si_{0.12})_{13}$ compounds. *J. Magn. Magn. Mater.* **2003**, *262*, 427–431.
57. Fujita, A.; Fujieda, S.; Fukamichi, K. Control of Magnetocaloric Effects by Partial Substitution in Itinerant-Electron Metamagnetic $La(Fe_xSi_{1-x})_{13}$ for Application to Magnetic Refrigeration. *IEEE Trans. Magn.* **2009**, *45*, 2620–2625. [CrossRef]
58. Fujita, A.; Fujieda, S.; Fukamichi, K. Changes in electronic states and magnetic free energy in $La_{1-z}Ce_z(Fe_xSi_{1-x})_{13}$ magnetic refrigerants. *J. Phys. D Appl. Phys.* **2011**, *44*, 064013. [CrossRef]
59. Fujieda, S.; Fujita, A.; Fukamichi, K. Enhancements of magnetocaloric effects in $La(Fe_{0.90}Si_{0.10})_{13}$ and its hydride by partial substitution of Ce for La. *Mater. Trans.* **2004**, *45*, 3228–3231. [CrossRef]
60. Fujieda, S.; Fujita, A.; Fukamichi, K.; Hirano, N.; Nagaya, S. Large magnetocaloric effects enhanced by partial substitution of Ce for La in $La(Fe_{0.88}Si_{0.12})_{13}$ compound. *J. Alloys Compd.* **2006**, *408*, 1165–1168. [CrossRef]
61. Shen, B.G.; Sun, J.R.; Hu, F.X.; Zhang, H.W.; Cheng, Z.H. Recent Progress in Exploring Magnetocaloric Materials. *Adv. Mater.* **2009**, *21*, 4545–4564. [CrossRef]
62. Shen, J.; Li, Y.X.; Sun, J.R.; Shen, B.G. Effect of R substitution on magnetic properties and magnetocaloric effects of $La_{1-x}R_xFe_{11.5}Si_{1.5}$ compounds with R=Ce, Pr and Nd. *Chin. Phys. B* **2009**, *18*, 2058–2062.
63. Gebara, P.; Kovac, J. Magnetocaloric effect of the $LaFe_{11.2}Co_{0.7}Si_{1.1}$ modified by partial substitution of La by Pr or Ho. *Mater. Des.* **2017**, *129*, 111–115. [CrossRef]

64. Gebara, P.; Kovac, J. The influence of partial substitution of La by Dy on structure and thermomagnetic properties of the $LaFe_{11.0}Co_{0.7}Si_{1.3}$ alloy. *J. Magn. Magn. Mater.* **2018**, *454*, 298–303. [CrossRef]
65. Fujieda, S.; Fujita, A.; Fukamichi, K.; Yamazaki, Y.; Iijima, Y. Giant isotropic magnetostriction of itinerant-electron metamagnetic $La(Fe_{0.88}Si_{0.12})_{13}H_y$. *Appl. Phys. Lett.* **2001**, *79*, 653–655. [CrossRef]
66. Chen, Y.F.; Wang, F.; Shen, B.G.; Wang, G.J.; Sun, J.R. Magnetism and magnetic entropy change of $LaFe_{11.6}Si_{1.4}C_x$ (x = 0–0.6) interstitial compounds. *J. Appl. Phys.* **2003**, *93*, 1323–1325. [CrossRef]
67. Rosca, M.; Balli, M.; Fruchart, D.; Gignoux, D.; Hill, E.K.; Miraglia, S.; Ouladdiaf, B.; Wolfers, P. Neutron diffraction study of $LaFe_{11.31}Si_{1.69}$ and $LaFe_{11.31}Si_{1.69}H_{1.45}$ compounds. *J. Alloys Compd.* **2010**, *490*, 50–55. [CrossRef]
68. Phejar, M.; Paul-Boncour, V.; Bessais, L. Investigation on structural and magnetocaloric properties of $LaFe_{13-x}Si_x(H,C)_y$ compounds. *J. Solid State Chem.* **2016**, *233*, 95–102. [CrossRef]
69. Gebara, P.; Cesnek, M.; Bednarcik, J. Anomalous behavior of thermal expansion of α-Fe impurities in the $La(Fe,Co,Si)_{13}$- based alloys modified by Mn or selected lanthanides (Ce, Pr, Ho). *Curr. Appl. Phys.* **2019**, *19*, 188–192. [CrossRef]
70. Paul-Boncour, V.; Nakouri, K.; Bessais, L. Optimization of Magnetocaloric Properties of Ball-Milled $La(Fe,Co,Si)_{13}(H,C)_y$. In Proceedings of the TMS 2019 148th Annual Meeting and Exhibition, San Antonio, TX, USA, 10–14 March 2019.
71. Mandal, K.; Pal, D.; Gutfleisch, O.; Kerschi, P.; Müller, K. Magnetocaloric effect in reactively-milled $LaFe_{11.57}Si_{1.43}H_y$ intermetalic compounds. *J. Appl. Phys.* **2007**, *102*, 053806. [CrossRef]
72. Zhao, J.L.; Shen, J.; Hu, F.X.; Li, Y.X.; Sun, J.R.; Shen, B.G. Reduction of magnetic hysteresis loss in $La_{0.5}Pr_{0.5}Fe_{11.4}Si_{1.6}H_x$ hydrides with large magnetocaloric effects. *J. Appl. Phys.* **2011**, *107*, 113911. [CrossRef]
73. Li, J.Q.; Liu, F.S.; Ao, W.Q.; Zhuang, Y.H.; Zhou, K.W. Influence of carbon on the giant magnetocaloric effect of $LaFe_{11.7}Si_{1.3}$. *Rare Met.* **2006**, *25*, 556–561. [CrossRef]
74. Wang, Z.C.; He, L.H.; Cuevas, F.; Shen, M.L.J.; Wang, F.W. Hydrogenation, structure and magnetic properties of $La(Fe_{0.91}Si_{0.09})_{13}$ hydrides and deuterides. *Chin. Phys. B* **2011**, *20*, 067502. [CrossRef]
75. Baumfeld, O.L.; Gercsi, Z.; Krautz, M.; Gutfleisch, O.; Sandeman, K.G. The dynamics of spontaneous hydrogen segregation in $LaFe_{13-x}Si_xH_y$. *J. Appl. Phys.* **2014**, *115*, 203905. [CrossRef]
76. Krautz, M.; Skokov, K.; Gottschall, T.; Teixeira, C.S.; Waske, A.; Liu, J.; Schultz, J.L.; Gutfleisch, O. Systematic investigation of Mn substituted $La(Fe,Si)_{13}$ alloys and their hydrides for room-temperature magnetocaloric application. *J. Alloys Compd.* **2014**, *598*, 27–32. [CrossRef]
77. Piazzi, M.; Bennati, C.; Curcio, C.; Kuepferling, M.; Basso, V. Modeling specific heat and entropy change in $La(Fe\text{-}Mn\text{-}Si)_{13-}H$ compounds. *J. Magn. Magn. Mater.* **2016**, *400*, 349–355. [CrossRef]
78. Morrison, K.; Sandeman, K.G.; Cohen, L.F.; Sasso, C.P.; Basso, V.; Barcza, A.; Katter, M.; Moore, J.D.; Skokov, K.P.; Gutfleisch, O. Evaluation of the reliability of the measurement of key magnetocaloric properties: A round robin study of $La(Fe,Si,Mn)H_\delta$ conducted by the SSEEC consortium of European laboratories. *Int. J. Refrig. Rev. Int. Froid* **2012**, *35*, 1528–1536. [CrossRef]
79. Mu, L.; Huang, J.; Zhang, W.; Liu, C.; Wang, G.; Zhao, Z. Influence of partial substitution of cerium for lanthanum on magnetocaloric properties of $La_{1-x}Ce_xFe_{11.44}Si_{1.56}$ and their hydrides. *J. Rare Earth* **2014**, *32*, 1135–1139. [CrossRef]
80. Hai, X.Y.; Mayer, C.; Colin, C.V.; Miraglia, S. In-situ neutron investigation of hydrogen absorption kinetics in $La(Fe_{1-x}Si_x)_{13}$ magnetocaloric alloys for room-temperature refrigeration application. *J. Magn. Magn. Mater.* **2016**, *400*, 344–348. [CrossRef]
81. Hai, X.Y.; Porcher, F.; Mayer, C.; Miraglia, S. Structural effects in the interstitial solid solution system $(La,Ce)(Fe,Si)_{13}C_xH$: Correlation with hydrogenation kinetics. *J. Appl. Phys.* **2018**, *123*, 7. [CrossRef]
82. Xia, W.; Huang, J.; Sun, N.; Lui, C.; Ou, Z.; Song, L. Influence of powder bonding on mechanical properties and magnetocaloric effects of $La_{0.9}Ce_{0.1}(Fe,Mn)_{11.7}Si_{1.3}H_{1.8}$. *J. Alloys Compd.* **2015**, *635*, 124–128. [CrossRef]
83. Sun, N.; Zhang, Y.; Zhao, X.; Guo, J.; Cheng, J.; Huang, J.; Zhang, Z. Microstructure, mechanical and magnetocaloric properties of bulk $La_{0.9}Ce_{0.1}Fe_{11.7-x}Mn_xSi_{1.3}$ hydrides prepared by high-hydrogen-pressure sintering,. *J. Magn. Magn. Mater.* **2020**, *495*, 165889. [CrossRef]
84. Brown, G.V. Magnetic heat pumping near room-temperature. *J. Appl. Phys.* **1976**, *47*, 3673. [CrossRef]
85. Rowe, A.; Tura, A. Experimental investigation of a three-material layered active magnetic regenerator. *Int. J. Refrig.* **2006**, *29*, 1286–1293. [CrossRef]
86. Balli, M.; Sari, O.; Zamni, L.; Mahmed, C.; Forchelet, J. Implementation of $La(Fe, Co)_{13-x}Si_x$ materials in magnetic refrigerators: Practical aspects. *Mater. Sci. Eng. B Adv.* **2012**, *177*, 629–634. [CrossRef]
87. Tusek, J.; Kitanovski, A.; Poredos, A. Geometrical optimization of packed-bed and parallel-plate active magnetic regenerators. *Int. J. Refrig.* **2013**, *36*, 1456–1464. [CrossRef]
88. Legait, U.; Guillou, F.; Kedous-Lebouc, A.; Hardy, V.; Almanza, M. An experimental comparison of four magnetocaloric regenerators using three different materials. *Int. J. Refrig.* **2014**, *37*, 147–155. [CrossRef]
89. Pulko, B.; Tusek, J.; Moore, J.D.; Weise, B.; Skokov, K.; Mityashkin, O.; Kitanovski, A.; Favero, C.; Fajfar, P.; Gutfleisch, O.; et al. Epoxy-bonded La-Fe-Co-Si magnetocaloric plates. *J. Magn. Magn. Mater.* **2015**, *375*, 65–73. [CrossRef]
90. Vasile, C.; Muller, C. Innovative design of a magnetocaloric system. *Int. J. Refrig.* **2006**, *29*, 1318–1326. [CrossRef]
91. Forchelet, J.; Zamni, L.; El Alami, S.E.; Hu, J.; Balli, M.; Sari, O. Corrosion behavior of gadolinium and La-Fe-Co-Si compounds in various heat conducting fluids. *Int. J. Refrig.* **2014**, *37*, 307–313. [CrossRef]

92. Aprea, C.; Greco, A.; Maiorino, A.; Masselli, C. Analyzing the energetic performances of AMR regenerator working with different magnetocaloric materials: Investigations and viewpoints. *Int. J. Heat Technol.* **2017**, *35*, S383–S390. [CrossRef]
93. Aprea, C.; Greco, A.; Maiorino, A.; Masselli, C. The environmental impact of solid-state materials working in an active caloric refrigerator compared to a vapor compression cooler. *Int. J. Heat Technol.* **2018**, *36*, 1155–1162. [CrossRef]